Naval Surface Warfare Center
Carderock Division
West Bethesda, MD 20817-5700

NSWCCD-50-TR-2003/022 July 2003

Hydromechanics Directorate

Technical Report

FlexTAC: An Advanced Submarine Control Surface and Actuation System

by

Scott Gowing, Bernie Carpenter, YuTai Lee, Paisan Atsavapranee and David Hess

MAJOR CARDEROCK DIVISION TECHNICAL COMPONENTS

CODE	011	Director of Technology
	10	Machinery Systems/Programs and Logistics Directorate
	20	Ship Systems and Programs Directorate
	50	Hydromechanics Directorate
	60	Survivability, Structures and Materials Directorate
	70	Signatures Directorate
	80	Machinery Research and Development Directorate
	90	Machinery In-Service Engineering Directorate

CARDEROCK DIVISION, NSWC, ISSUES THREE TYPES OF REPORTS:

1. **CARDEROCKDIV reports, a formal series,** contain information of permanent technical value. They carry a consecutive numerical identification regardless of their classification or the originating directorate.

2. **Directorate reports, a semiformal series,** contain information of a preliminary, temporary, or proprietary nature or of limited interest or significance. They carry and alphanumerical identification issued by the originating directorate.

3. **Technical memoranda, an informal series,** contain technical documentation of limited use and interest. They are primarily working papers intended for internal use. They carry an identifying number which indicates their type and the numerical code of the originating directorate. Any distribution outside CARDEROCKDIV must be approved by the head of the originating directorate on a case-by-case basis.

NDW-DTRC 5602/51 (Rev. 9-94)

REPORT DOCUMENTATION PAGE

Form Approved
OMB No. 0704-0188

1. AGENCY USE ONLY *(Leave Blank)*	2. REPORT DATE	3. REPORT TYPE AND DATES COVERED
	July 2003	Final, Juy 2003

4. TITLE AND SUBTITLE
FlexTAC: An Advanced Submarine Control Surface and Actuation System

5. FUNDING NUMBERS
Sponsor Order:
N0002402WR10228/AA
Appropriation: 1721319
Subhead: 84RJ
Program Element: 0603561N
JO: 02-1-5050-107

6. AUTHOR(S)
Scott Gowing, Bernie Carpenter, YuTai Lee, Paisan Atsavapranee and David Hess

7. PERFORMING ORGANIZATION NAME(S) AND ADDRESS(ES)
Propulsion and Fluid Systems Department, Code 5400
NSWC, Carderock Division
9500 MacArthur Blvd.
West Bethesda, MD 20817-5700

8. PERFORMING ORGANIZATION REPORT NUMBER
NSWCCD-50-TR-2003/022

9. SPONSORING / MONITORING AGENCY NAME(S) AND ADDRESS(ES)
Naval Sea Systems Command (NAVSEA)
Advanced Submarine Technology Office
93R

10. SPONSORING / MONITORING AGENCY REPORT NUMBER

11. SUPPLEMENTARY NOTES

12.a DISTRIBUTION / AVAILIBILITY STATEMENT
Unlimited Distribution

12.b DISTRIBUTION CODE

13. ABSTRACT ***(Maximum 200 words)***

An electrically-actuated flexible tab was tested on a model of a submarine sternplane comprised of a fixed stabilizer with a hinged flap. The tab was built into the trailing edge of the flap and was tested for its ability to control overall lift and reduce the torque required to rotate the flap itself. Shape memory alloy wires, embedded in a flexible silicone compound along the length of the tab, pulled on the tab's rear edge to curl it to one side or the other. The fixed portion (stabilizer) and flap were mounted on balances that measured the six forces and moments on each of those sections to measure the overall and individual element forces. These tests were performed in the 36-inch Water Tunnel at the Naval Surface Warfare Center, Carderock Division, over a range of angles of attack and flap that are typical of submarine operations. In addition to the effect of the tab on the flap torque and overall sternplane performance, the electrical power and response rates of the wire actuators were measured along with the contour of the flexible tab while under load. The predictions of a numerical control surface optimization scheme using two RANS codes were compared to the experimental results to test the code's fidelity.

This report presents the experimental results, describes the design of the SMA actuators and their control system, and presents the CFD calculations of the sternplane characteristics using the numerical optimization scheme.

16. SUBJECT TERMS			15. NUMBER OF PAGES
FLAPS AERODYNAMIC CONTROLS SHAPE MEMORY ALLOY TABS			36
			16. PRICE CODE
17. SECURITY CLASSIFICATION OF REPORT	18. SECURITY CLASSIFICATION OF THIS PAGE	19. SECURITY CLASSIFICATION OF ABSTRACT	20. LIMITATION OF ABSTRACT
UNCLASSIFIED	UNCLASSIFIED	UNCLASSIFIED	SAME AS REPORT

(THIS PAGE INTENTIONALLY LEFT BLANK)

CONTENTS

FIGURES

TABLES

NOMENCLATURE

c	Mean chord length
C_l	Lift coefficient, $\frac{L}{\frac{1}{2}\rho V^2 c^2}$
C_q	Torque coefficient, $\frac{Q}{\frac{1}{2}\rho V^2 c^3}$
L	Sternplane lift
Q	Flap torque
V	Water velocity
x	Chordwise location
δ	Tab displacement
ν	Kinematic viscosity
ρ	Mass density

(THIS PAGE INTENTIONALLY LEFT BLANK)

ABSTRACT

An electrically-actuated flexible tab was tested on a model of a submarine sternplane comprised of a fixed stabilizer with a hinged flap. The tab was built into the trailing edge of the flap and was tested for its ability to control overall lift and reduce the torque required to rotate the flap itself. Shape memory alloy wires, embedded in a flexible silicone compound along the length of the tab, pulled on the tab's rear edge to curl it to one side or the other. The fixed portion (stabilizer) and flap were mounted on balances that measured the six forces and moments on each of those sections to measure the overall and individual element forces. These tests were performed in the 36-inch Water Tunnel at the Naval Surface Warfare Center, Carderock Division, over a range of angles of attack and flap that are typical of submarine operations. In addition to the effect of the tab on the flap torque and overall sternplane performance, the electrical power and response rates of the wire actuators were measured along with the contour of the flexible tab while under load. The predictions of a numerical control surface optimization scheme using two RANS codes were compared to the experimental results to test the code's fidelity.

This paper presents the experimental results, describes the design of the SMA actuators and their control system, and presents the CFD calculations of the sternplane characteristics using the numerical optimization scheme.

ADMINISTRATIVE INFORMATION

The work described in this report was performed by three groups: the Propulsion and Fluid Systems Department (Code 5400) and the Maneuvering and Control Department (Code 5600) of the Hydromechanics Directorate at the Naval Surface Warfare Center, Carderock Division (NSWCCD), and the Lockheed Martin Astronautics - Space Systems. The work was funded by the Naval Sea Systems Command (NAVSEA), Advanced Submarine Technology Office, SUB-RT3 as part of the Flexible Tab-Assisted Control Task (FlexTAC) of the 6.4 Maneuvering and Control R&D Program, under work unit number 1-5050-107.

INTRODUCTION

HISTORICAL OVERVIEW

Tabs attached to the rear edge of flaps have been used for many years in the aviation industry to trim an aircraft's flight attitude, serve as a fine control, reduce flap actuation torque, or control the flap entirely ("servo mode"). The first application of a secondary control surface to the primary control surface appears to have been the invention of the 'Flettner' rudder, which was basically a flap on the rear edge of an all-moveable rudder. Steering was performed by moving the flap that rotated the freely-rotating rudder. Control of the flap required less torque than that required for rotating the rudder itself. This concept was applied to ship rudders as early as 1921 (Figure 1) and was used either as a servo control on a freely-rotating rudder, or in a linked configuration to balance the rudder actuation torque [1]. Flettner rudders were also used on British airplanes in the mid 1920s [2]. In addition to lower torques, these rudders reacted less to ship motions and seaways because they were free to deflect, and the reactions on the steering mechanisms were not as harsh. The disadvantages of these rudders were sluggish response at slow speeds, requirement of retaining a mechanical control system for the primary rudder in the event of a flap failure, and dynamic instabilities caused by inertial accelerations that tended toward unbalanced hydrodynamic loads. The addition of a secondary flap onto a wing, or a tab onto a primary flap, was also used to simply trim an aircraft in flight by providing a separate control scheme independent of the primary controls [2]. This is the major use of tabs today, although some tabs are still used as servo controls on flaps with strict requirements on their design to avoid dynamic instabilities [3]. Present marine applications of rudders with servo flaps primarily involve steering systems for towed barges or other bodies, for which pilots are absent [4], [5].

Figure 1 Ship rudder with Flettner flap (1921)

RECENT DEVELOPMENTS

In marine applications, flaps used on control surfaces (submarine control surfaces, large ship rudders) must be well-balanced to avoid extreme torque requirements for rotation. Balance is

achieved by placing the flap shaft aft of the leading edge (typical submarine design), or using a flap planform that has an overhang projecting forward of the shaft (horn design). An alternative or auxiliary approach to controlling the flap or reducing torque actuation requirements is by the use of a tab connected to the flap's rear edge. These advantages, along with others, were researched in some recent programs that led to the experimental effort described in this report.

The present tab design is an outgrowth of two parallel efforts: the Advanced Control Surface (ACS) program under the Office of Naval Research (ONR), and the Smart Aircraft and Marine Propulsion System Demonstration (SAMPSON) program under the Defense Advanced Research Projects Agency (DARPA). In the late 1980s, the DARPA Subtech Program sponsored a series of studies on a number of advanced control surface concepts. These preliminary works showed that tab-assisted control (TAC for short) has many advantages over a conventional flapped control surface: reduced power requirements (50-90% power reduction for flap actuation), improved reliability through increased redundancy, and up to 30% more lift than can be achieved with the flap alone. However, development of a viable tab actuating system presents many challenges. One of the above DARPA-sponsored studies tallied potential challenges and graded several state-of-the-art actuating technologies for TAC implementation [6].

In 1993, Synthesis and Processing of Intelligent Cost Effective Structures (SPICES) was initiated under another DARPA program, with the aim of developing and demonstrating cost effective design, fabrication, assembly, and control methods for smart structures and systems [7]. The first phase of SPICES produced encouraging results in vibration reduction using a smart materials mount [8]. Continued investigation in the second phase identified high payoff areas for the application of smart-structures technology to aerospace and naval systems [9]. These preliminary works led to SAMPSON, which aimed to demonstrate the successful adaptation of shaped memory alloy (SMA) technology to specific aerospace and marine applications. The use of SMA materials for tab actuation allowed a compact design that could fit entirely inside the existing control surface envelope, yet offer enough power to actuate the tab using electricity alone.

Before developing an SMA-actuated tab, the control forces, moments and actuation torque requirements for a modern submarine sternplane with a simple hinged tab attached to the flap were measured for a wide range of operating parameters. Figure 2 shows the tab-assisted control (TAC) sternplane model tested in the 24 in water tunnel at NSWCCD in 1998. This was a scale model of a Virginia class sternplane fitted with Partial Span Flaps (PSF). The tab, with a chord length of 10% of the sternplane mean chord, was hinged on the rear edge of the flap. These tests showed the following advantages of using a tab attached to the flap as compared to a flap-only configuration [10]:

1. The tab can augment the maximum lift from maximum flap deflection to achieve greater control authority at low speed. At the maximum flap angle (27 degrees), 30 degrees of tab increases the control surface lift the same amount as 6 degrees of flap deflection in the linear region.
2. The tab can be used to reduce the lift of a jammed flap. The lift with a flap jammed at 27 degrees can be reduced to the lift of a 15 degree jammed flap by deflecting that flap's tab in the opposite direction. This enables residual lift control at forward speed using the non-jammed flap (for a PSF configuration).
3. The torque required to either hold the flap in position, or overcome the bearing friction and move the flap, can be attained at all speeds with tab deflections of 20 degrees or less. Using the tab in this fashion decreases the sternplane lift only a small amount at low flap angles and angles of attack. At high attack and flap angles, using the tab this way reduces the control surface lift by almost one-half.
4. The tab can be used by itself at high speed as fine control for control surface lift, although the resultant drag is greater using only the tab versus the flap for the same amount of lift.

These results encouraged the testing of the present sternplane model using SMA technology for tab actuation and building the tab out of flexible material formed into the back face of the rigid flap.

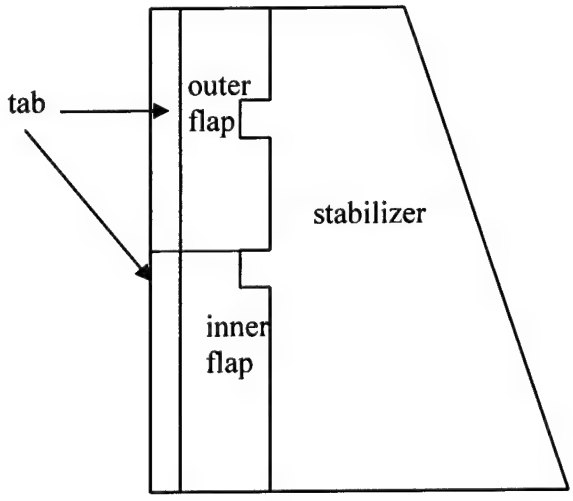

Figure 2 Tab Assisted Control (TAC) sternplane model tested in 24" water tunnel

The tab model that was tested in this experimental effort was built under a NAVSEA Advanced Submarine Technology (SUB-RT) program with the objective of quantification of the advanced sternplane's performance using a flexible, shape memory alloy (SMA)-actuated tab at the trailing edge of a flap.

It is most desirable for the actuating system for the trailing edge tab to be housed within the flap, where the limited volume available makes conventional actuators impractical. In that context, a SMA actuator becomes a prime contender due to its compactness and its simple power delivery mechanism. In applications where noise could be a concern, the SMA actuator is also very quiet compared to many of the conventional actuators. Integrating the tab as a flexible part of the flap trailing edge instead of making a separate hinged element avoids gap leakage flows and their associated noise and detrimental effects on flap lift. This flexible, SMA-actuated tab design is denoted Flexible Tab-Assisted Control (FlexTAC).

36" WATER TUNNEL TEST SETUP

STERNPLANE/FLEXTAC MODEL

The sternplane model was a $1/8^{th}$ scale copy of the Virginia class Scheme I design, except that no gudgeons were used to connect the flap to the stabilizer, and the flap was a single, full-span flap. The stabilizer and flap portions were independently mounted to shafts through strain-gaged balances for load measurements. Figure 3 shows the model and groundboard setup.

Table 1 lists the model dimensions and hydrodynamic characteristics. The green, flexible tab section had a length in the flow direction that was 10% of the sternplane's mean chord, and the tab was a continuous extension of the flap surface, with no hinges or gaps. Numerous SMA wires were embedded inside the flap and tab assembly and pulled on a rigid piece in the tab's trailing edge to bend the tab in the shape of a smooth curve. The tab extended along the entire span of the flap.

A sand trip turbulent stimulator was installed on the stabilizer to insure turbulent flow at the mean Reynolds number of 1.55×10^6. Figure 4 shows the inside of the flap and an end view of the flexible tab under deflection.

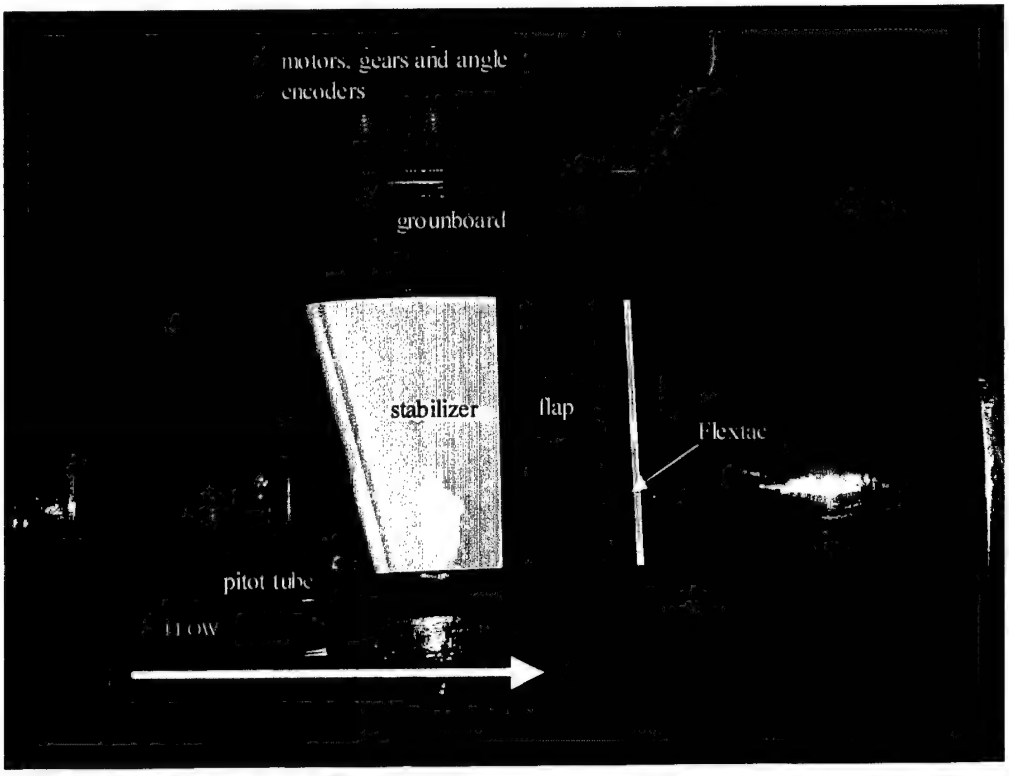

Figure 3 Sternplane model in 36" water tunnel

Table 1. Dimensions of FlexTAC sternplane model.

Dimension	Length (inches)	% mean chord
Root chord	22.13	
Tip chord	17.45	
Mean chord	19.79	
Span	17.49	
Taper ratio	0.79	
Flap chord	9.45	47.7
Flap stock location (re trailing edge)	6.30	31.8
Tab chord	2	10.1
Sweep angle	11.4 degs	
Root NACA section	0018	
Tip NACA section	0018	

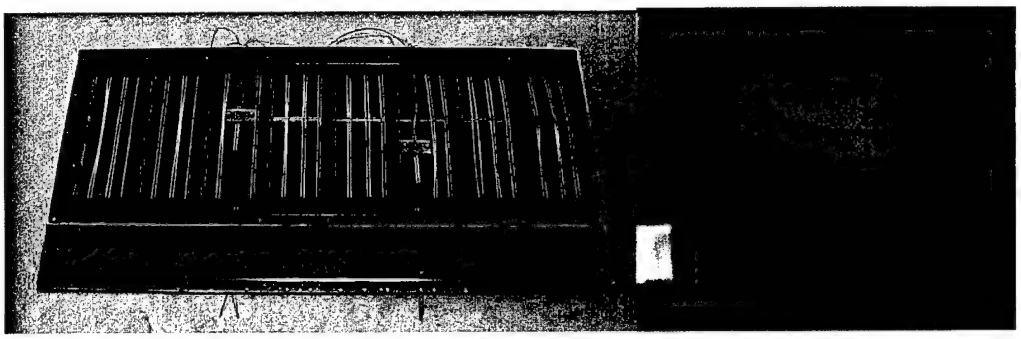

Figure 4 Internal flap construction and side view of deflected tab

FLEXTAC CONSTRUCTION

The construction of the aluminum flap and attached flexible tab is shown in Figure 4. The pliable, green silicone casting adhered to a glass epoxy center laminate that formed the centerplane of the tab. The laminate was clamped into the aluminum flap along the forward edge and attached to a plastic tailpiece along the rear edge. Steel wires tied to the tailpiece ran through the silicone and were attached in series to the SMA wires within the flap cavity. These wires, in turn, were anchored in the front of the flap cavity and connected to the electrical leads that ran out of the flap and tunnel to the control electronics. This arrangement was built into both sides of the flap. Encapsulating the steel wires inside the silicone kept the SMA wires inside of the flap cavity for easy access if any repairs were required. Contraction of the wires on one side pulled the tailpiece, causing the tab to curl in the desired direction. Antagonistic operation of the shape memory wires on the opposite side provided a fail-safe "power-off" neutral position and a balanced level of control on both sides of the neutral position. The mechanical stiffness of the center laminate maintained a neutral control position and minimized power consumption. By balancing actuator strains and power, a desired tab deflection could be maintained under adverse hydrodynamic loading and ambient cooling conditions. In addition to the wires, two Linear Variable Displacement Transducers (LVDTs) were fitted into each side of the flap to measure tab displacement and provide feedback to the SMA wire control system.

SMA WIRE DESIGN

Because the shape memory effect is a temperature-dependent phenomenon, the application of Nickel-Titanium (NiTi) SMA wires required that its transition temperature be higher than the maximum expected exposure temperature. For FlexTAC, a NiTi alloy with a transition temperature of 80°C was selected. Total motion requirements of FlexTAC were related to the length of shape memory wire that could be installed within the geometric confines of the

flap cross-section. Selection of wire size depended strongly on termination techniques because the terminations are typically three times the wire size, yet they still had to fit within the envelope of the flap geometry. A wire diameter of 0.02-in. was selected to enable terminations within the flexible edge region where section thickness limited the length of shape memory wire that could be accommodated. Although control surface displacement could be increased with higher actuator prestrain in the wire, the resultant penalty was a shorter fatigue life. A wire strain of 2% was selected for this design. The wire actuation had to supply sufficient force to overcome the structural stiffness of the laminate and the compression/extension of the pliable silicone in addition to load resulting from hydrodynamic forces. Based on previous designs having similar dimensions and hydrodynamic loads, a target of 15 lbs was selected for the wire force, within the 17 to 20 lbs force capability of 0.02-in. diameter SMA wire. Approximately 70 individual wires were installed on each side of the 17 in span of the FlexTAC flap.

TAB CONTROL SYSTEM

Antagonistic actuation was used to balance the wire actuator forces to maintain the desired tab deflection. A general electrical description of the antagonistic control is shown in Figure 5. The control system modified the current flow to the SMA actuators that in turn regulated their temperature via. resistive heating. Commanded tip displacement signals were input as user-defined set-points. An error signal was generated from the difference between the set-point and the measured FlexTAC tip displacement, and a PID (proportional-integral-differential) control algorithm then calculated the required power output signal based on the magnitude of the error signal.

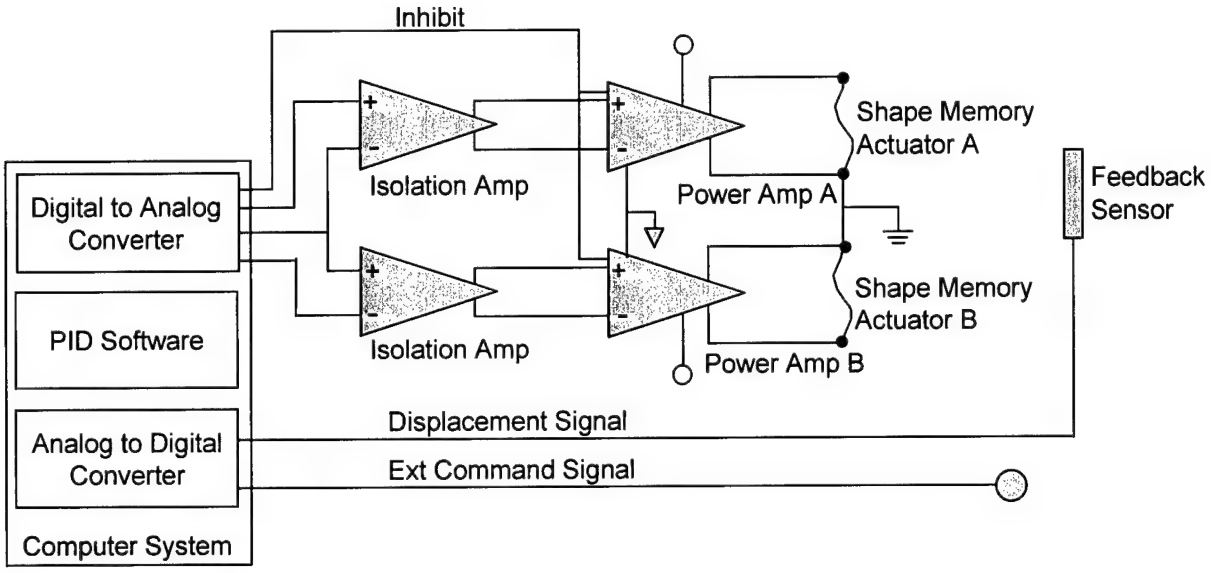

Figure 5 SMA Actuator Control System

These calculations were performed at a rate of 2000 to 5500 Hz depending on graphical update requirements. The resulting output controlled a programmable DC power supply that regulated current flow to the specified shape memory wire circuit. The power supplies updated their output at a rate of 750 Hz, or approximately 100 times faster than the response rate of FlexTAC. In addition to the commanded tab position, a small amount of power was run through the wires to heat them slightly and remove wire slack.

MODEL MOUNTING, OPERATION AND LOAD MEASUREMENT

The model was mounted to a groundboard fitted into the upper part of the open jet test section of the 36 in. water tunnel as shown in Figure 3. The resulting flow cross-section, circular except for the groundboard, was 29 in. high by 36 in. wide with an upstream area contraction ratio of 9.8 to 1. The entire sternplane model was mounted to a 30 in. circular cutout in the groundboard that rotated to change the angle of attack, and the flap was mounted with its own circular cutout for independent flap rotation. These rotations were controlled by DC gearmotors that engaged large gears fixed to the ends of the shafts to which the stabilizer and flap were mounted. Two AMTI model ZMC1-5-500 strain-gaged balances measured all six components of the stabilizer and flap forces. These balances had 250 lb force capacities in the lift and drag directions, and 100 in-lb capacities for all the moments. They were selected for their sensitivity for measuring flap torque reductions, compactness, and availability. Figure 6 shows one of the two balances, and Figure 7 shows the residual errors of the balance calibrations. The angle of attack and flap angle were measured by calibrated voltage variations from 10-turn potentiometers

attached to the stabilizer shaft and flap shaft drive gears. The flow speed was measured with a 10 psi differential pressure transducer attached to a pitot-static tube inserted into the open-jet flow. The data were recorded on a Pentium laptop using software written in LABVIEW®.

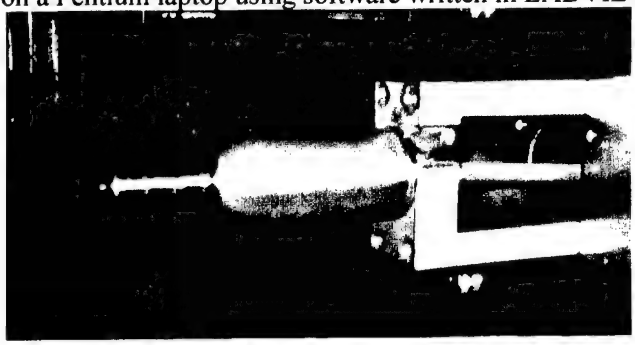

Figure 6 Balance (mounted to calibration fixture)

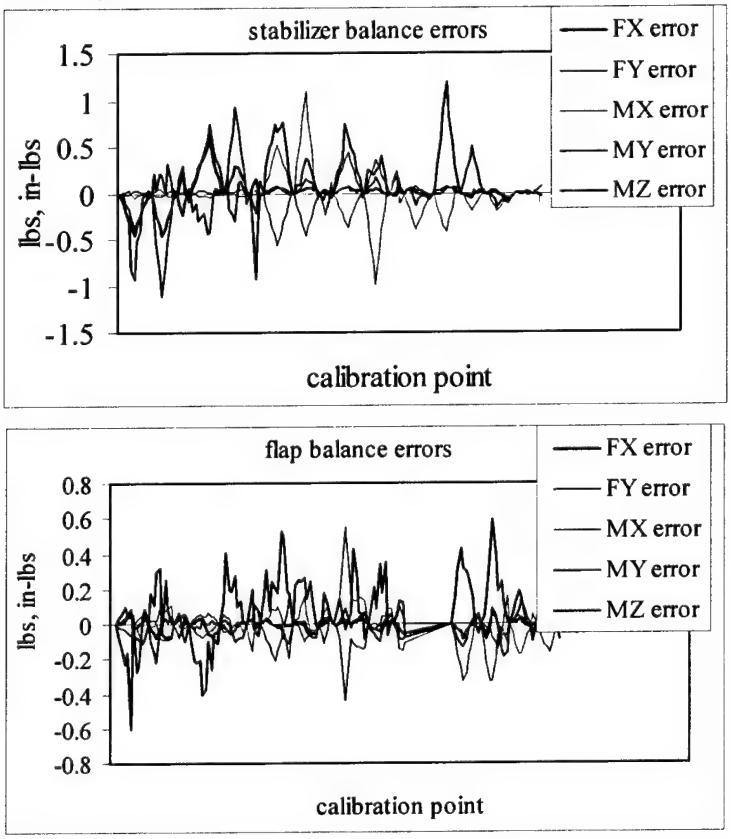

Figure 7 Balance errors

FLEXTAC CONTOUR MEASUREMENTS

An Accuity Model AR600-8 laser sensor was used to measure the contour and displacement of the flexible tab under running conditions. This was done to check the shape and symmetry of the deflected tab in addition to the LVDT data for their single attachment points. The laser sensor triangulated the diffuse reflection of a laser beam off the tab into an adjacent CCD line scan camera to measure the distance to the tab, and this sensor was traversed along the streamwise direction to map the contour of the tab from the rigid end of the metal flap all the way to the tab's trailing edge. The accuracy of the measurement is nominally 0.008 inches. These measurements were done on only the flap's port side. Figure 8 shows the profiles of the deflected FlexTAC tab, with the tab trailing edge on the right. The x-axis is the non-dimensional chordwise location on the tab with x/c=1.00 being the trailing edge. The y-axis represents the tip displacement relative to the neutral position, in units of deflection/chord or δ/c. The maximum tab deflection was between 0.58 in. on one side and 0.54 in. on the other, or about 3% of the mean chord. The tab measurements were repeated at two locations along the span, but the distance between these locations was small as a result of limited access. The results were very similar at the two span locations.

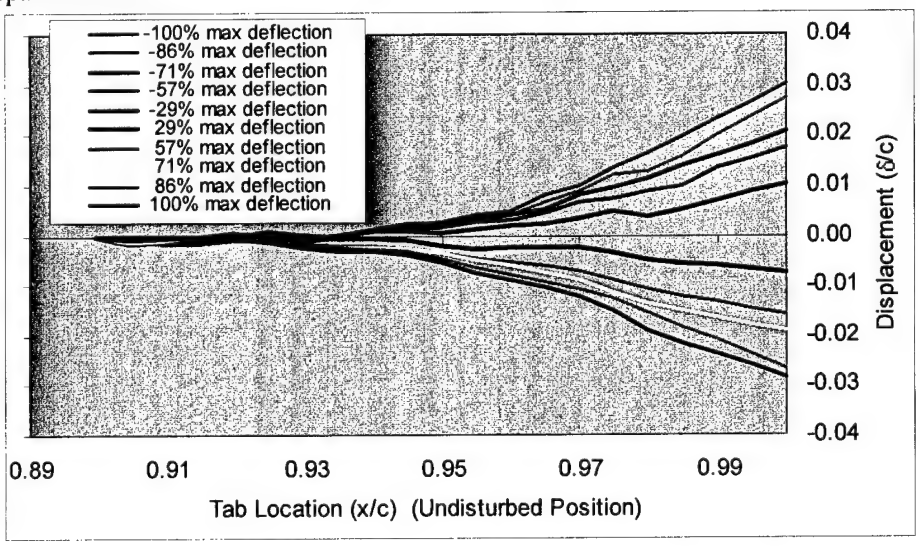

Figure 8 Typical FlexTAC contour measured by laser sensor

FLOW QUALITY, BLOCKAGE, AND WALL CORRECTIONS

Blockage and wall corrections were determined in three steps using standard vortex image techniques [11]. There were no weight tares to be concerned with because the balance rotated with the model. The dynamic pressure was corrected for blockage effects of both the

model and the model's wake. The drag was further corrected for the change in induced drag incurred from the downwash. Finally, the angle of attack was corrected for the downwash and the curvature of the streamlines relative to the ¼ chord point. The angle corrections were relatively large, with a downwash correction that was 9.0% of the geometric angle, and a streamline curvature correction that was an additional 2.3% of that angle. The net angle of attack correction was 11.3% for lift derived from angle of attack. There was no correction to the flap angle or tab angle. For cases of lift from large flap deflections, the change in the angle of attack was significant, as much as 20%, simply because the flap-induced changes in lift produced downwash angles that were large compared to the small angles of attack. This change in attack angle was properly accounted in the flap lift curve by adding the lift coefficient $(dC_l/d\alpha)*d\alpha$. The net blockage effects of the model (and its wake) on velocity were 1.5% to 2.0% for the whole range of attack and flap angles.

REYNOLDS EFFECTS

The test program was conducted at a nominal speed of 8.2 ft/sec, yielding a Reynolds number of 1.29×10^6 based on the mean chord. A minimum Reynolds number of 1.0×10^6 is typically used as a guideline for wing tests to be insensitive to Reynolds effects [12]. The addition of the sandstrip also assured turbulent flow over the model. The speed was not varied during the tests except for two runs to examine the electrical power consumption as the flow dynamic pressure and loading was increased. These runs varied speed from 4.0 ft/sec to 12.7 ft/sec.

TEST PROGRAM

Table 2 shows the stabilizer and flap angles and tab deflections tested through the test program. Preliminary tests measured the basic hydrodynamic performance of the sternplane assembly, followed by tests of the effect of FlexTAC tab deflection on overall lift and flap torque for various combinations of flap and stabilizer angle. The initial tests involved smaller deflections than later tests to minimize the risk of preliminary failure from broken wires. The last few tests measured the power consumption of the actuators to both overcome the mechanical resistance of the flexible tab and to withstand varying hydrodynamic loading at constant deflection.

Table 2 Test parameters

Angle of attack α (degs)	Flap angle δ (degs)	Tab deflection (δ/C)	Test
-8 to 8	0	0	$dC_l/d\alpha$
0, 3, 6	-27 to 27	0	$dC_l/d\delta$
0	0	0.0123 to –0.0126	$dC_l/d\delta_t$
0	10	0.0127 to –0.0126	$dC_l/d\delta_t$
0	20	0.0130 to –0.0131	$dC_l/d\delta_t$
0	-5	0.0222 to –0.0222	$dC_l/d\delta_t$
0	-15	0.0190 to –0.0222	$dC_l/d\delta_t$
0	-25	0.0000 to –0.0222	$dC_l/d\delta_t$
6	0	0.0125 to –0.0125	$dC_l/d\delta_t$
6	20	0.0129 to –0.0126	$dC_l/d\delta_t$
6	-20	0.0127 to –0.0125	$dC_l/d\delta_t$
0	0	0.0199 to –0.0215	Flextac response rate
0	0	0.0222 to –0.0222	Flextac tab profile, power consumption
0	0	0.0222 to –0.0222	hydrodynamic loading power consumption

EXPERIMENTAL RESULTS

LIFT FROM ANGLE OF ATTACK (FLAP AND TAB AT ZERO)

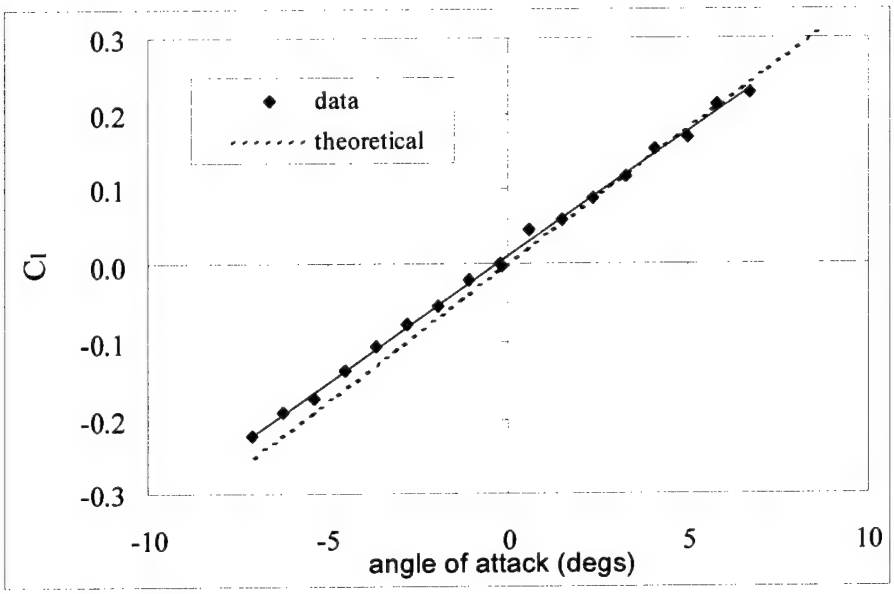

Figure 9 Lift from angle of attack

The lift of the entire model at angles of attack (flap and tab at 0) is shown in Figure 9. The lift-curve slope based on mean chord^2 is 0.0328/degree, 8.1% lower than the theoretical lift-curve slope of 0.0358/degree predicted by thin wing theory for an elliptical foil of similar area and planform [13]. Previous wind tunnel tests on a similar planform NACA0015 wing show a lift-curve slope of 0.0354/degree at the same Reynolds number [12]. Previous tests of a 1/16 scale model of this sternplane in another water tunnel had a lift curve slope of 0.0361[10]. The reason for the discrepancy of the present data is unclear, although the blockage effects in this test were about twice those of the tests in the 24 in. water tunnel [10]. The angle correction in that test was only 5% versus 11% for the present tests.

LIFT FROM FLAP DEFLECTION (STABILIZER AND TAB AT ZERO)

The lift of the sternplane with pure flap deflection and zero tab deflection is shown in Figure 10. The lift increases to flap angles of 20 degrees and then drops off at higher angles. The average of data from 9 flapped wings with overhung flap designs similar to this control surface, and with similar aspect ratios, is also shown [14]. The flap overhang is the portion of the flap forward of the shaft axis. The measured flap lift performance is 0.0209 for flap angles to 15 degs, and this is 6% lower than the flap lift measured in the 1/16 scale tests in the 24in water tunnel

[10]. The reason for this discrepancy is unknown. Runs 7 and 13 are repeated runs to check the data repeatability.

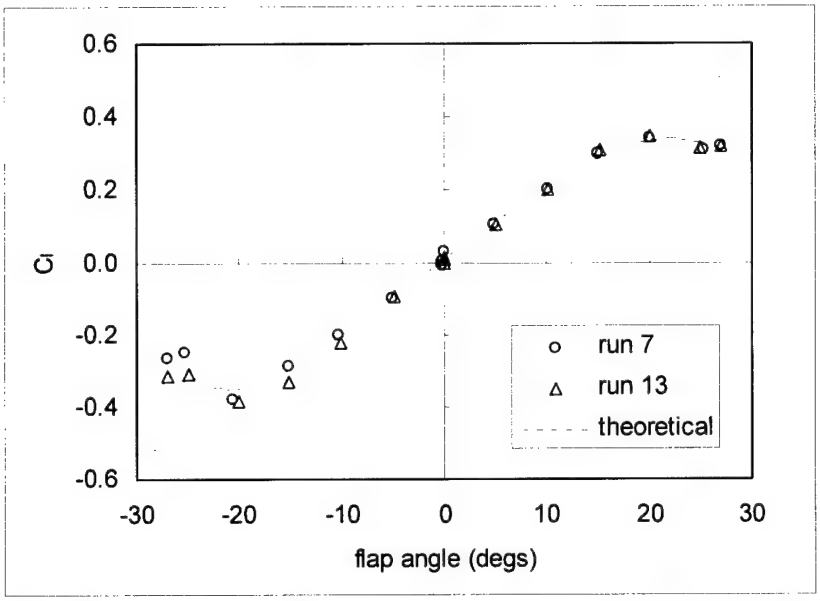

Figure 10 Comparison of theoretical and measured flap lift

LIFT WITH PURE TAB DEFLECTION (STABILIZER AND FLAP AT ZERO)

The lift caused by the flexible tab deflection alone is shown in Figure 11. This comparison shows how the lift from the flexible tab compares to that of a hinged tab of similar chord [15,16]. For comparison purposes, the flexible tab angular deflection is defined as the arc tangent of the trailing edge tab displacement divided by the tab chord in the neutral position. The flexible tab lift-curve slope is 0.009/deg, almost *twice* the theoretical value of 0.0048 for a hinged tab modeled as a plain flap of the same chord. The lift curve slope of the hinged tab tested at 1/16 scale was 0.0049/deg, confirming the plain-flap theoretical value [10]. A possible explanation of the increased tab effectiveness is its trailing edge tangent angle. Examination of the deflected tab profile (Figure 4) shows the tab curves mostly over the aft half of the tab, and the trailing edge angle is roughly *twice* that predicted for a rigid hinged tab of the same chord rotated to the same trailing edge deflection. This benefit may be a result of the continuous camber of the FlexTAC design versus a hinged tab. Comparison of the lift curve slopes show the tab-induced lift to be 45% of the flap-induced lift for the same angular deflection, and 29% of the lift induced from similar changes in angle of attack. Thus the lift is very sensitive to modifications to the trailing edge flow, and this increased performance of the curved shape of the flexible tab versus the straight tab is significant. The flexible tab can then be used as an effective means of lift

enhancement for more maneuverability, or as a means of reducing lift on a jammed Partial Span Flap, enabling different casualty recovery techniques.

For the rest of the report, the tab deflection will be expressed in terms of tip deflection normalized on mean chord (δ_t/C).

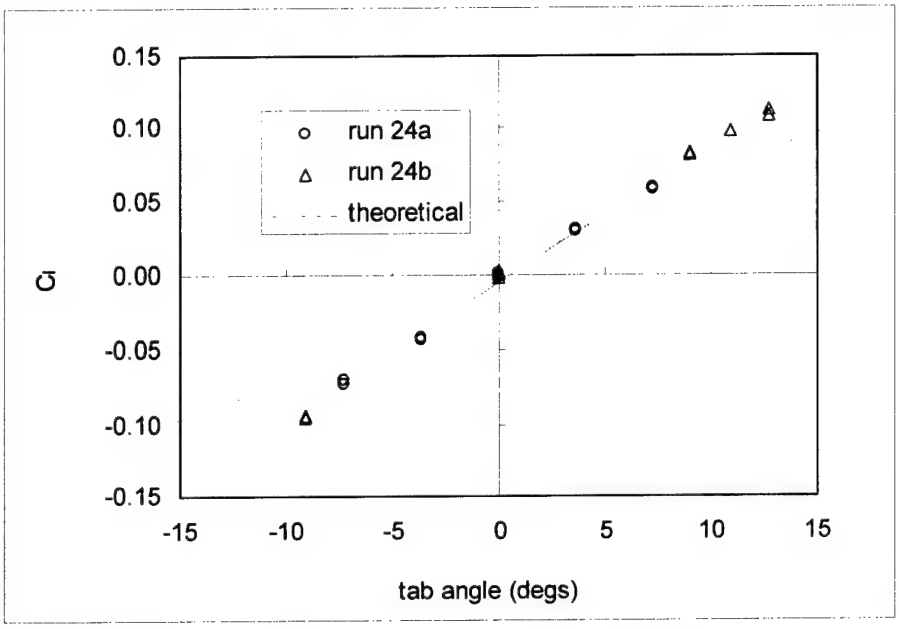

Figure 11 Lift from FLEXTAC tab deflection

TAB INFLUENCE ON FLAP TORQUE

Of prime importance in this experiment is the measurement of the ability of the tab to reduce the torque required to deflect the flap (torque reduction mode) or even control the flap entirely (Flettner mode). Figure 12 shows the influence of the tab deflection on flap torque for 11 flap angles at zero degrees angle of attack. The flap angles have been corrected for blockage effects and hence they are not equal to the input control values. The tab influence on torque is linear for all flap angles tested, even up to angles of almost 25 degs. Figure 13 shows a similar influence for three flap angles at six degrees angle of attack. All the curves do not have the same tab deflection because the precise impact of hydrodynamic loading on the SMA wires was initially unknown, and the initial runs used small deflections to minimize the chance of wire breakage. Regardless, in all the runs that were conducted except one, a tab deflection (δ_t/c) of less than 0.022 was sufficient to drive the flap torque to zero. For the –24.9 deg flap angle at 0 degs attack angle, it appears that the flap torque would have been zero had the tab displacement been increased. Figure 14 shows the sensitivity of flap torque to tab angle (the slopes of the data in Figure 12 and Figure 13) as a function of flap angle for both angles of attack, and these plots

shows an increase in torque sensitivity at the more extreme flap angles. The average change in flap torque coefficient with tab deflection is 2.62 ($dC_q/d(\delta_t/c)$). To compare this control sensitivity to the sensitivity of the flap torque to flap angle for small angle rotations, the tab deflection can again be expressed in angular units as before. The variation of flap torque with tab deflection is 0.00457 per tab deg. The flap torque variation with flap angle is –0.00133 per flap degree. Hence the sensitivity of the flap torque to tab angle is over three times greater than the sensitivity of flap torque to small flap angles. This is a simple consequence of the attachment of the tab at the flap's trailing edge where it exerts the greatest leverage on flap torque.

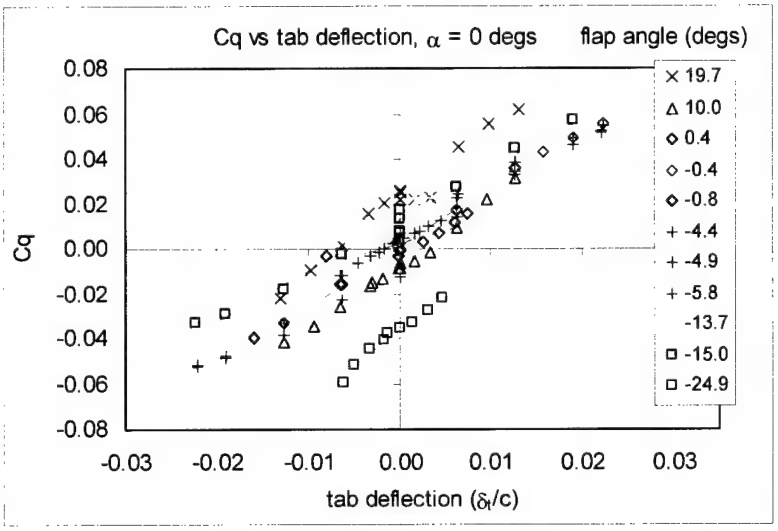

Figure 12 Tab effect on flap torque at 0 degs angle of attack

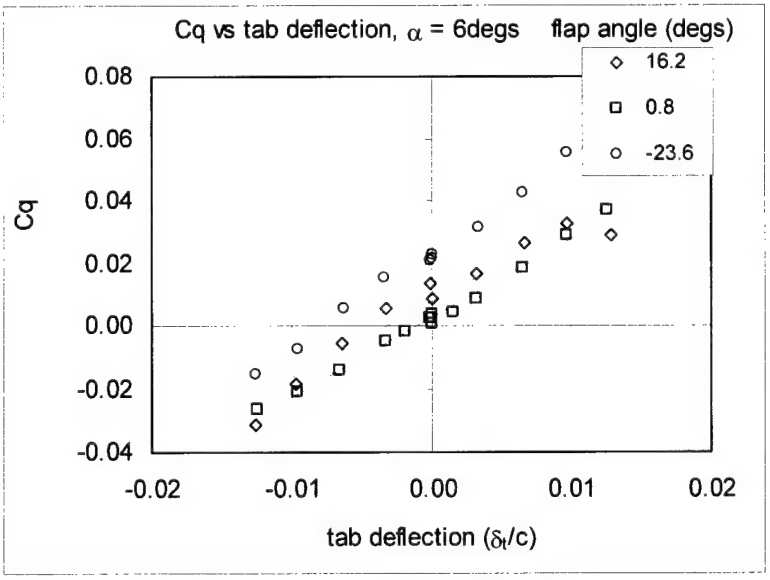

Figure 13 Tab effect on flap torque at 6 degs angle of attack

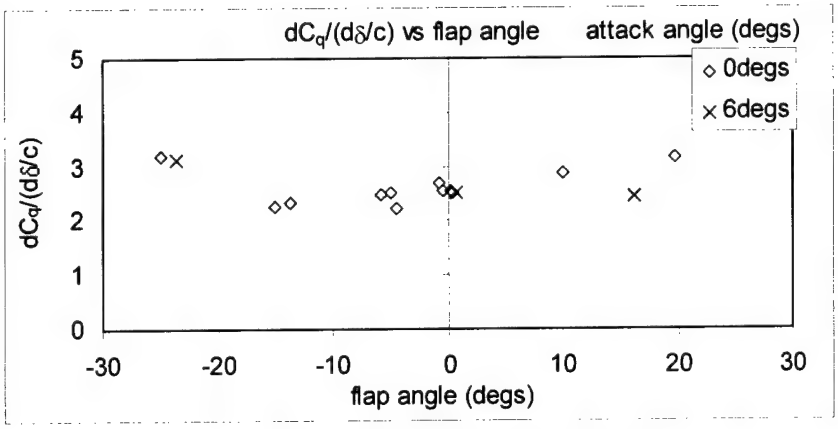

Figure 14 Tab influence on flap torque

TAB INFLUENCE ON LIFT

While the influence of tab deflection on lift has been demonstrated, this effect must be linear and repeatable over the spectrum of angles of attack and flap typical for a submarine sternplane, as shown for the tab influence on flap torque. Figure 15 shows the influence of the tab deflection on overall lift for 11 flap angles at zero degrees angle of attack. Again, the tab influence on lift is linear for all flap angles tested, even up to angles of almost 25 degs. Figure 16 shows a similar influence for 3 flap angles at six degrees angle of attack. Figure 17 shows the sensitivity of overall lift to tab angle (the slopes of the data in Figure 15 and Figure 16) as a function of flap angle for both angles of attack, and these plots also show an increase in lift sensitivity at the more extreme flap angles, similar to the increase in flap torque sensitivity to tab displacement at high flap angles.

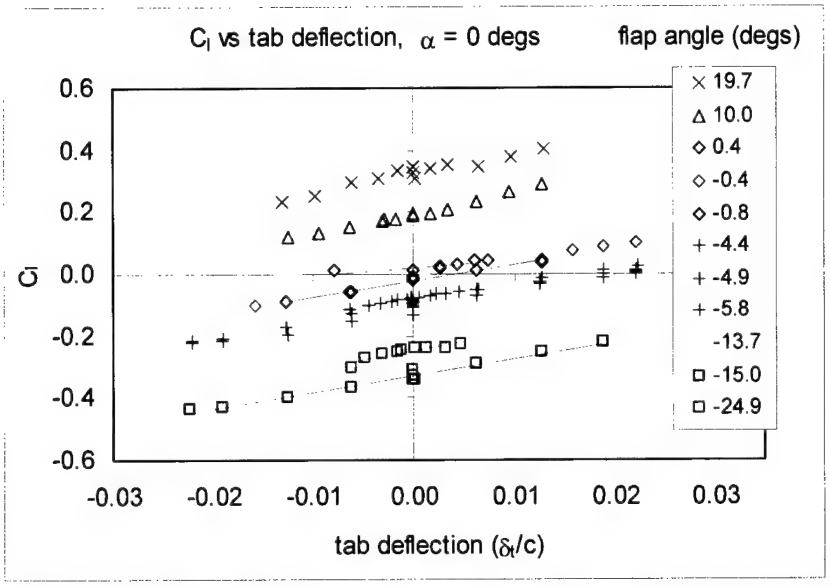

Figure 15 Tab effect on lift at 0 degs angle of attack

Comparing again the sensitivity of lift to equivalent tab angular rotation, the average change in lift coefficient is 0.0098 per tab degree, compared with 0.0209 per flap degree for changes in flap angle. Thus the tab lift authority is 47% of the lift authority of the flap for the same rotation angle.

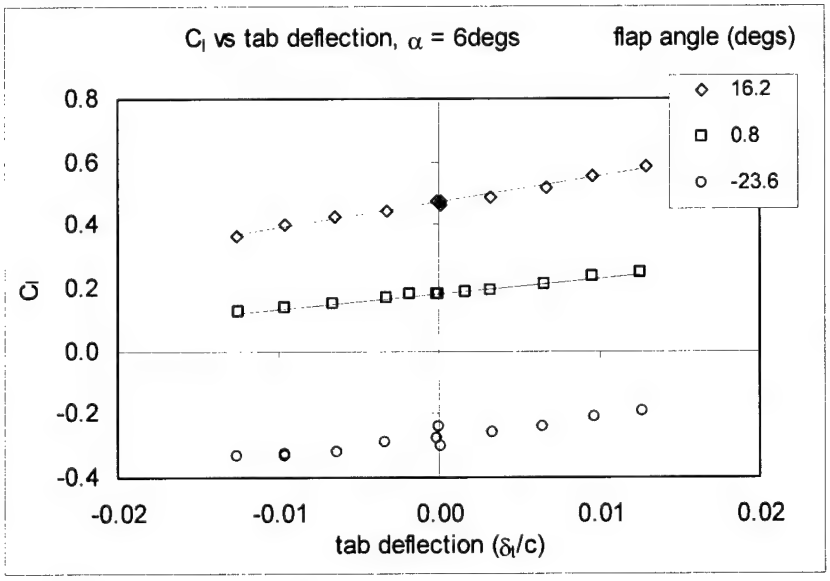

Figure 16 Tab effect on lift at 6 degs angle of attack

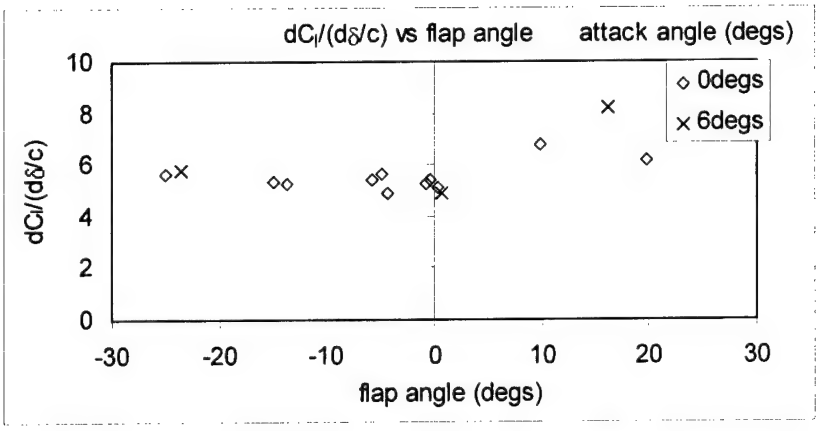

Figure 17 Tab effect on overall lift

TAB EFFECT ON LOCATION OF FLAP FORCES

The measured flap torque and flap side force were used to resolve the location of center of forces on the flap as a function of tab displacement. This position remained stationary on the flap chord over the range of tab motion tested. Figure 18 compares this measured chordwise location of the center of forces on the flap to the calculated value for a simple hinged flap of the same dimensions. The measured and theoretical force locations compare well, showing that the effect of the tab on the flap is well-behaved and there are no signs of flow separation or other issues.

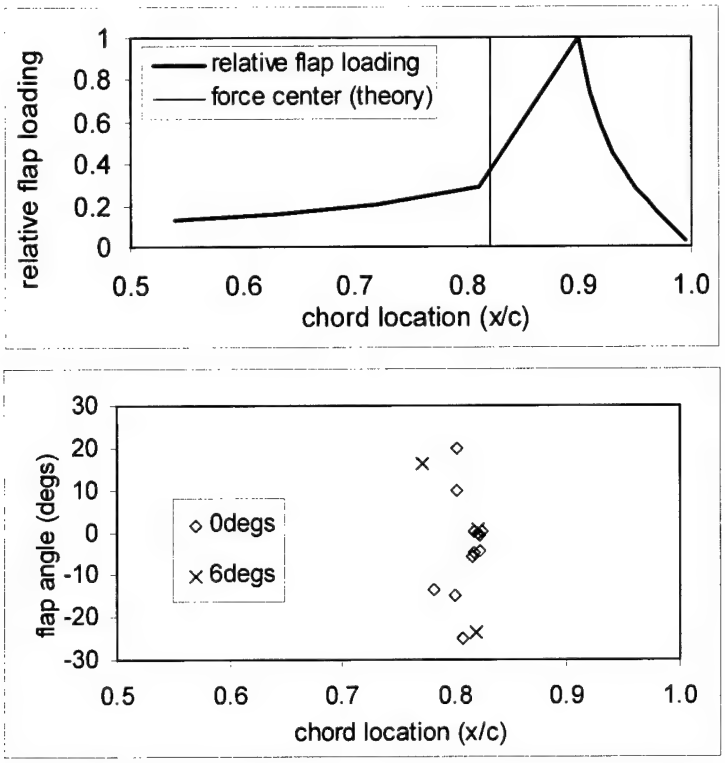

Figure 18 Center of flap forces with FlexTAC tab deflection

COMPUTATIONAL RESULTS

A computational effort was made in addition to the experimental program to further computational techniques for improving control surfaces. The ultimate computational goal is a numerical optimization procedure to design multi-element control surface shapes that provide better maneuvering capabilities under given system constraints. Towards this end, a Direct Method for Optimization (DMO) [17] has been developed that maximizes (or minimizes) an objective (or an output) function that represents the parameter of interest from a mathematical model of the problem. An example of the objective function would be a composite function of combined lift and torque. The referenced DMO has been used for achieving an optimal diffuser shape for a shipboard air-conditioning compressor using a structured-grid RANS calculation and gradient scheme for the optimization computations. Adapting this DMO to a multi-element control surface requires an unstructured CFD scheme that accommodates gap geometry and grid movement by a regridding process that iteratively marches to an optimal shape.

Before the shape optimization can proceed, one must have faith in the predictive capabilities of the computations. Thus, the initial goal during this experiment was to carefully

validate the prediction ability of unstructured CFD calculations using the results of the FlexTAC model. Previous comparisons of computational results from this program with the TAC model tests run in the 24" water tunnel showed discrepancies that could have been caused by differences between the physical and gridded model. Specifically, the tested model had gudgeons along 17% of the flap/stabilizer joint that were absent in the gridded model. The FlexTAC model had no gudgeons and allowed a better comparison to the computational model. No computations were made for the deflected tab shape because this shape was unknown ahead of time, and the flap and stabilizer deflections were sufficient in themselves to validate the predictive model. The undeflected shape of the flexible tab was assumed to be rigid for the validation effort and the displacement data of the laser device showed this assumption to be reasonably accurate for the non-deflected cases.

COMPUTATIONAL SCHEMES AND GRIDS

Two computational approaches were used to investigate the predictive DMO capabilities for the FlexTAC model. Both approaches perform RANS calculations on a computational domain extending 2 chord lengths upstream and 4.5 chords downstream of the model, 3 chord lengths in the transverse direction, and 2 chord lengths in the spanwise direction.

The first RANS approach used the unstructured UNCLE code [18]. UNCLE solves the incompressible Navier Stokes equations with artificial compressibility. The flow solver is a node-centered, finite volume, implicit time-marching scheme, and the flow variables are stored at the vertices. A one-to-one mapping converts the edge information to the faces of the control volumes. UNCLE is programmed for parallel processing, using MPI for interprocessor communication and a coarse-grained domain decomposition for concurrent solution within subdomains assigned to multiple processors. A two-equation q-ω turbulence model [19] is used for the present work.

The grids used for the UNCLE calculations are generated using an advancing normal methodology for the boundary layer elements and an advancing front/local reconnection (AFLR) methodology [20] for the isotropic tetrahedral elements. Surface grid generation and geometry preparation were accomplished using SolidMesh [21]. Special attention was paid to the grid spacing in the gap between the stabilizer and the flap to avoid poor grid quality. A symmetry boundary condition is applied on the plane formed by the root section of the model and a far-field boundary condition is employed at a sufficient distance to avoid any influence on the solution.

The second RANS approach uses the unstructured CRUNCH code [22],[23] developed by CRAFT Tech, Inc. The solver uses a finite-volume Roe/TVD flux construction based on the cell-vertex formulation. The code works for multi-element grids including tetrahedral,

hexahedral, prismatic and pyramid cells. CRUNCH is programmed for parallel processing, using MPI and an automated load balancing domain decomposition. A dynamic grid capability, which is essential for future optimization of the control surfaces, uses a node movement solver for automated embedding and sliding interfaces. A two-equation k-ε turbulence model with a wall function approach is used for the current calculations.

The grids used for the CRUNCH calculations were generated using GRIDGEN. They consist of approximately 2.5 million hexahedral cells. The outer domains are treated with far-field boundary conditions.

The pre-test calculations were performed at a nominal speed of 10 ft/s and a Reynolds number of 1.833×10^6. The test was later performed at a lower speed of 8.5 ft/s because of load limits on the balances. The test conditions were $\alpha = 0$ with $\delta_F = -20, 0, 10$, and 20 degs. Since the profile shapes of the flexible portion of the FlexTAC airfoil were not known beforehand, the predictions assumed it to be rigid.

COMPUTATIONAL RESULTS

The comparisons are plotted in Figure 19 and Figure 20. The predicted FlexTAC lift and drag values are in relatively good agreement with the experimental values. Also shown are comparisons of the earlier data from the TAC experiments that used a sternplane model similar to FlexTAC except with smaller size scale and with gudgeons at the stabilizer/flap joint. The measured FlexTAC drag at $\alpha = \delta_F = \delta_T = 0$ is 0.0162. When normalized on planform area, this coefficient becomes 0.0183 and is very close to experimental values for flapped rudders with similar flap chord and balance ratios [25]. Figure 20 shows the stabilizer and flap torque comparisons, again for both FlexTAC and the TAC experiments. The CFD predictions correctly capture the trend of the flap torque to have a maxima and minima with flap deflection in the absence of gudgeons, as was tested in FlexTAC, and the torque magnitudes are also well-predicted. The TAC model had gudgeons over 13% of the stabilizer/flap joint that were not modeled in the CFD predictions, and these gudgeons would have had an impact on the flow over the flap, as shown in the experimental data. This is why the flap torque in the TAC experiments did not have a maxima and minima as was measured in FlexTAC or predicted by the CFD codes.

The computational efforts summarized here represent some of the highlights of the overall CFD effort. Greater details of the computations, optimization, and gridding schemes are discussed in a separate report [25].

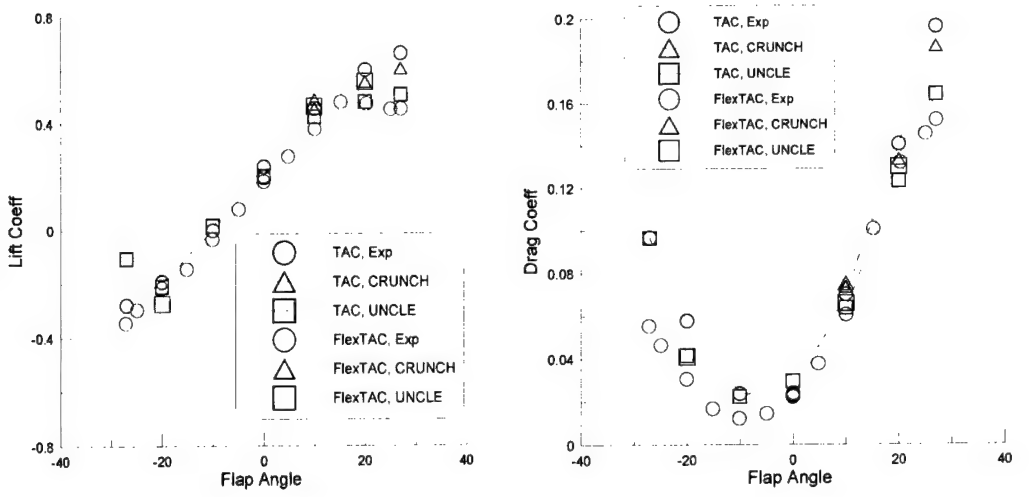

Figure 19 Lift and drag comparisons

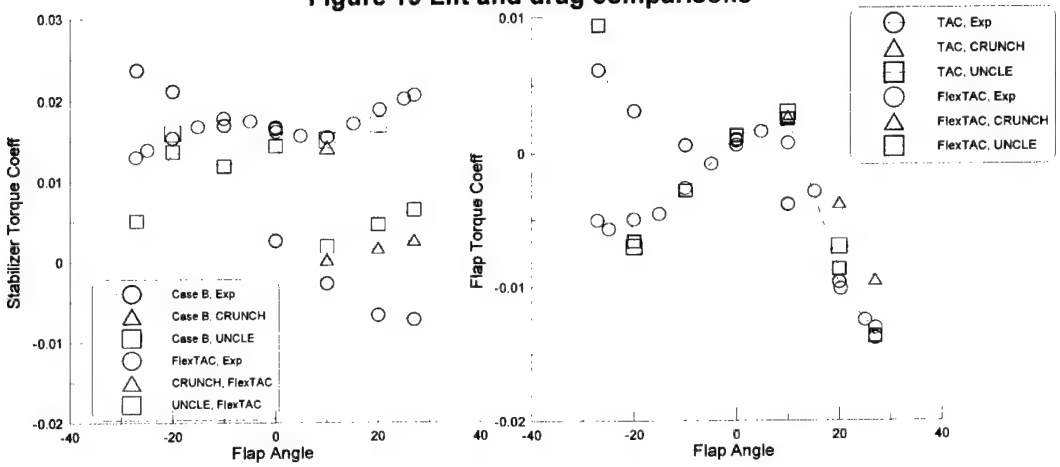

Figure 20 Stabilizer and flap torque comparisons

FLEXTAC CHARACTERISTICS

FLEXTAC RESPONSE RATE

The response rate of the SMA-actuated tab was measured by applying full power to one side of the tab to obtain a large deflection, letting it cool for a short time with power off, then applying power to the other side, and repeating the process. Figure 21 shows the response rate as a function of time. The average tab deflection rate on an angular basis is 1.33 degs/sec during the powered phase of the test. It is difficult to compare this rate to full-scale flap rotation rates because this SMA actuator is not representative of a final design that will be used at full-scale, but it is in the same order of magnitude as the present flap rate of 7 degs/sec.

FLEXTAC POWER CONSUMPTION

The power required by the SMA wires to deflect the flexible tab must overcome the deformation resistance of the tab material and the hydrodynamic loading on the tab itself. A test was conducted to differentiate between these two requirements by holding the tab at constant deflection or angle and ramping up the tunnel speed. The power required to initially deform the tab with no speed is the power used for material deformation, and the change in power with speed is the power to sustain hydrodynamic loads. Figure 22 shows the results. The power required to deflect the tab at zero speed was 244 watts. Increasing the speed to 12.6 ft/sec (flow dynamic pressure of 156 psf) increased the power consumption to only 262 watts, hence the increase in power to overcome hydrodynamic loads was only 7% of the original power used to deflect the material. Thus the material deformation is the main source of power consumption for this flexible tab design, and there appears to be some hysteresis in the demand as the deformation is reduced. Figure 23 shows the power consumption for varying amounts of deformation or tab angle, and the power demand is linear.

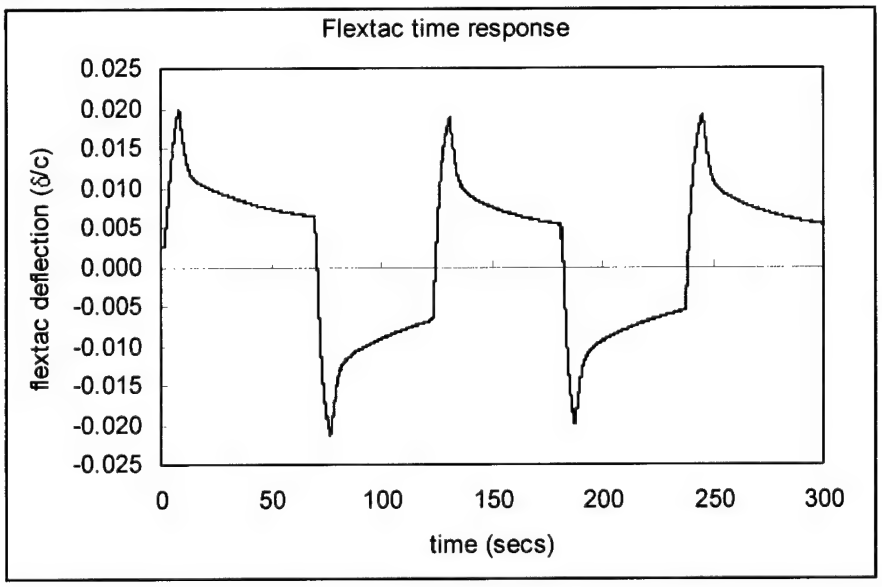

Figure 21 FLEXTAC response rate with intermittent cooling

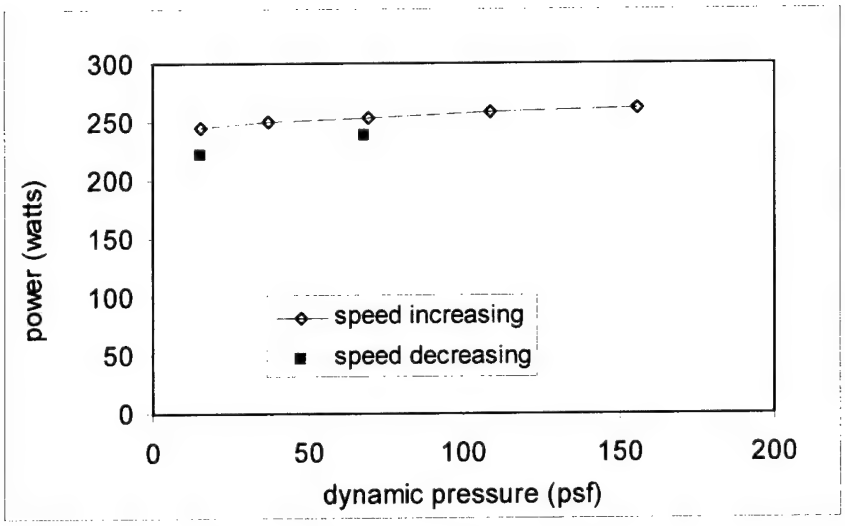

Figure 22 Power for hydro loading

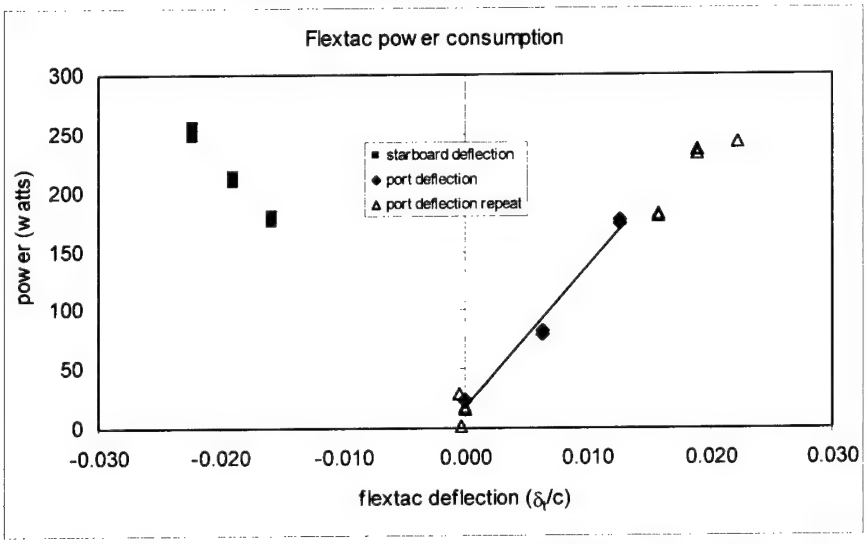

Figure 23 Power required to deflect flexible tab

CONCLUSIONS

A multi-element control surface has been developed that uses shape memory alloy wire actuators to bend the flap trailing edge and assist flap operation in the same way as a tab. Reduced flap actuation torque and extra lift control are realized with all-electric actuators that require very little space. The contour of the flexible flap trailing edge is a smooth curve yet the hydrodynamic forces on the flap are greater than forces induced by a simple hinged tab. The

variations of overall lift and flap torque with tab deflection are linear with tab deflection and nearly independent of angles of attack and flap, enabling simple control. Tab trailing edge movement of less than 3% of the sternplane's mean chord is sufficient to drive the flap actuation torque to zero for flap angles to 25 degrees and angle of attack to 6 degrees.

The integrity of a computational optimization scheme has been tested using two different RANS codes and both results are close to the experimental values and trends. This scheme can be used to redefine a multi-component control surface towards an optimum parameter of performance.

The response rate of the actuators shows that the flexible tab can be deflected quickly in either direction. The electrical power required for actuation is governed mostly by the compressibility of the encapsulating flexible material and only a small portion of the power is needed to overcome hydrodynamic loading.

ACKNOWLEDGEMENTS

This report and the experimental program leading to it were made possible through the efforts and support of prior 93R program manager Doug Dahmer, and present SUB-RT3 manager Steve Weinstein. Many thanks to Rosa Lee whose persistence and patience has had a significant influence on seeing this report to completion. Thanks also go to Kirk Anderson for the water tunnel flow visualization efforts and to John Hamilton for his setup of the optical measurement of tab tip displacement.

INITIAL DISTRIBUTION

REFERENCES

1. Overgaard, O., and Livingston, J., "Recent Development of the Ship Rudder with Particular Reference to the 'Flettner Rudder'," Trans. Soc. Naval Arch. and Marine Eng., Vol. 34, 1926, p205.
2. Reid, E.G., "Servo Control Flaps," Jour. Aero. Sciences, Vol. 1, No. 4, Oct. 1934, p. 155.
3. Abramson, Jane, CD/NSWC Code 5600, private communication.
4. McKenzie, J.S., "Flap rudder and steering system," US Patent No. 4,944,239 July 1990.
5. Patrick, J.V., "Hawser Steering Anti-Yawing and Safety Mechanism for Towed Barges and the Like," US Patent No. 3,469,552 Sept 1969.
6. Carli, V. B., et al., "Flap-Assisted Control Surfaces (FACS) Ship Integration Study", General Dynamics, Electric Boat Division, July 1992.
7. Jacobs J. - "Synthesis and processing of intelligent cost effective structures: a final review of the ARPA SPICES program", Proceedings: Smart Structures and Materials 1996 - Industrial and Commercial Applications of Smart Structures Technologies, C. Robert Crowe, Vol. 2721, pp. 167-188, SPIE, San Diego, CA.
8. Dunne, J. and Jacobs J. - "Active vibration control testing of the SPICES program final demonstration article", Proceedings: Smart Structures and Materials 1996 - Industrial and Commercial Applications of Smart Structures Technologies, C. Robert Crowe, Vol. 2721, pp. 189-202, SPIE, San Diego, CA.
9. Dunne J. P., Jacobs S. W., and Baumann E. W. - "Synthesis and processing of intelligent cost effective structures phase II (SPICES II): smart materials aircraft applications evaluation", Proceedings: Smart Structures and Materials 1998 - Industrial and Commercial Applications of Smart Structures Technologies, Janet M. Sater, Vol. 3326, pp. 2-12, SPIE, San Diego, CA.
10. Nguyen, T. D., Gowing, S., and Bochinski, D., (1999) "Tab-Assisted Control Surface for Marine Application," presented at the International Symposium Warship '99 Naval Submarines 6.
11. Rae, W. H. and Pope A.: Low speed wind tunnel testing, John Wiley & Sons, Inc., 1984.
12. Whicker, L.G. and Fehlner L.F. - "Freestream Characteristics of a Family of Low-Aspect Ratio, All-Movable Control Surfaces for Application to Ship Design", David Taylor Model Basin Rept. No. 933, Dec. 1958.
13. Abbott, I. H. and Doenhoff A. E.: Theory of Wing Sections, Dover Publications, Inc., 1959.
14. Kerwin, J. E., Mandel P. and Lewis S. D. - "An experimental study of a series of flapped rudders", Journal of Ship Research, Dec. 1972.
15. Wilson, M. B., and Kerczek C. von - "An Inventory of Some Force Producers for Use in Marine Vehicle Control", Rept. DTNSRDC-79/097.

16. Young, A. D. - "The Aerodynamic Characteristics of Flaps", British Aeronautical Research Council R&M 2622, Feb. 1947.

17. Lee, Y. T., Luo, L., and Bein, T. W., (2001) "Direct Method for Optimization of a Centrifugal Compressor Vaneless Diffuser," Transactions of the ASME, J. of Turbomachinery, Vol. 123, Jan., pp. 73-80.

18. Hyams, D. G., Sreenivas, K., Sheng, C., Nichols, S., Taylor, L. K., Briley, W. R., Marcum, D. L., and Whitfield, D. L., (2002) "An Unstructured Multielement Solution Algorithm for Complex Geometry Hydrodynamic Simulations," presented at the 24th Sym. On Naval Hydrodynamics, Fukuoka, Japan, July 8-13.

19. Coakley, T. J., Hsieh, T., (1985) "A Comparison between Implicit and Hybrid Methods for the Calculation of Steady and Unsteady Inlet Flows," AIAA Paper 85-1125.

20. Marcum, D., and Weatherill, N. (1994) "Unstructured Grid Generation Using Iterative Point Insertion and Local Reconnection" *AIAA*, 33(9):1619-1625.

21. Gaither, J., Marcum, D., Mitchell, B. (2000) "SolidMesh: A Solid Modeling Approach To Unstructured Grid Generation." *7th International Conference on Numerical Grid Generation in Computational Field Simulations.*

22. Hosangadi, A., Lee, R. A., York, B. J., Sinha, N., and Dash, S. M., (1996) "Upwind Unstructured Scheme for Three-Dimensional Combusting Flows," *J. of Propulsion and Power*, Vol. 12, No. 3, May-June, pp. 494-503.

23. Ahuja, V., Hosangadi, A., Arunajatesan, S., (2001) "Simulations of Cavitating Flows Using Hybrid Unstructured Meshes," *J. of Fluids Engineering*, Vol. 123, No. 2, June, pp. 331-340.

24. T.R. Quackenbush, et al. - "Design, fabrication, and test planning for an SMA-actuated vortex wake control system", Proceedings: Smart Structures and Materials 1998 - Industrial and Commercial Applications of Smart Structures Technologies, Janet M. Sater, Vol. 3326, pp. 259-281, SPIE, San Diego, CA.

25. Lee, Y.T., Ebert, M., and Hjosangadi, A., "Flow Predictions for Multi-Element Control Surfaces", Rept. NSWCCD-50-TR–2002/061, December 2002

EXTERNAL DISTRIBUTION

ORGANIZATION	NAME (Copies)
NAVSEA	
SUB-RT	S. Weinstein (2)
	M. Stout (2)
ONR	
333	K. Kim (2)
333	P. Purtell (2)
333	R. Joslin (2)
DARPA	
TTO	S. Walker
LMA-SS	B. Carpenter (2)
EB	J. Hall
	J. Panosky
SCS	R. Shoaff
DTIC	(2)

CENTER DISTRIBUTION

CODE	NAME (Copies)
3421	NSWCCD Library
2630	D. Dahmer
5000	I. Koh
5060	D. Walden
5010	Code 5010
5200	W. Day
5300	J. Johnston
	J. Hamilton
5400	R. Szwerc
	M. Wilson
	S. Jessup
	M. Donnelly
	Y. Lee
5500	T. Applebee
5600	E. Ammeen
	J. Feldman
	D. Hess
	P. Atsvapranee
	D. Bochinski
	S. Cubbage
	M. Lee
	J. Abramson